# 74.38 Tb/s Transmission Over 6300 km Single Mode Fibre Enabled by C+L Amplification and Geometrically Shaped PDM-64QAM

Maria Ionescu, *Member, IEEE,* Domaniç Lavery, *Member, IEEE,* Adrian Edwards, Eric Sillekens, *Student Member, IEEE,* Daniel Semrau, *Student Member, IEEE,* Lidia Galdino, *Member, IEEE,* Robert I. Killey, *Senior Member, IEEE,* Wayne Pelouch, *Member, IEEE,* Stuart Barnes, and Polina Bayvel, *Fellow, IEEE*

*(Invited Paper)*

***Abstract*—Ultrawide-bandwidth optical amplification over almost 90 nm, covering the C+L bands, is described. Complemented by system-tailored geometrical constellation shaping and nonlinearity compensation, it enabled a record capacity transmission of 74.38 Tb/s over 6,300 km of G.654 single-mode fibre. The hybrid scheme, combining backward Raman pre-amplification with EDFA, significantly improves the average effective noise figure across the entire bandwidth, allowing the use of span lengths of 70 km. The system-tailored GS-64QAM constellation was optimised to both linear link impairments and transceiver nonlinearities, improving the gap to the AWGN channel capacity relative to square 64QAM from 0.6 bit/symbol to 0.35 bit/symbol. We experimentally evaluated the system performance using the bit-wise achievable information rate (AIR) and signal-to-noise ratio (SNR) at the end of transmission, as well as post SD-FEC BER.**

***Index Terms*—Broadband C+L band transoceanic transmission, Raman amplification, Erbium-doped fibre amplifier, nonlinear compensation, geometric constellation shaping.**

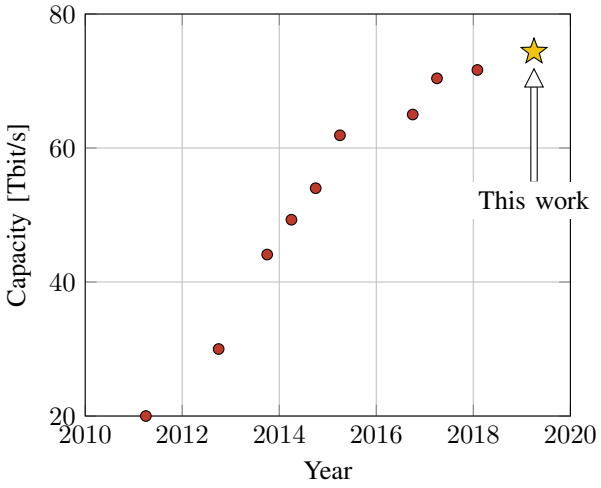


Fig. 1: Records of transoceanic transmission experiments over >5900km.

## I. Introduction

RECENT years have seen significant improvements in achievable information rates of single-mode fibres (SMF) by more than doubling the optical transmission band over optical fibres, extending beyond the C-band into the L-band [1]-[11] and even the S-band [12]. Wide-bandwidth amplification techniques combined with advanced digital signal processing (DSP) techniques and constellation shaping, have enabled new transmission records over transoceanic distances (>5,900 km). Notably, previous experimental demonstrations of 65 Tb/s over 6,600 km [9] and 71.65 Tb/s over 6,970 km [8] were achieved through the use of C- and L-band EDFA amplifiers, coded modulation and advanced nonlinear compensation (NLC) techniques. The work described in this paper demonstrates an improvement over previous records [1]-[10], as shown in Figure 1, achieved through improved amplifier design and modulation format, tailored to system impairments.

Whilst, at present, C-band EDFAs are the standard commercial amplifiers used in the deployment of subsea transmission systems, bandwidth extensions from the C-band into the L-band is possible by demultiplexing the signal over the two respective bands, separately amplifying with a dedicated C-band EDFA and an L-band EDFA, and finally multiplexing the two signals. This approach results in additional losses and a spectral gap of 4-6 nm between the two bands [7], [10]. Efforts have been directed towards the investigation of promising alternatives for both increasing the transmission bandwidth of deployed optical amplifiers and providing a seamless amplification bandwidth. Such alternatives include hybrid amplifiers based on EDFA and distributed Raman amplification (DRA) [6], [11] or semiconductor optical amplification (SOA) [12]. While SOA provides a continuous wide-bandwidth for a small form factor solution, its relatively high noise figure limits the maximum transmission distance. On the other hand, DRA has been one of the earliest amplification schemes [13] considered in optical telecommunications, due to its multiple advantages including wavelength-agnostic continuous broadband amplifi-

M. Ionescu was previously with Xtera, Bates House, Church Road, Romford, RM3 0SD, UK, currently with Nokia Bell Labs, Paris-Saclay, Nozay, 91620, France.

D. Lavery, E. Sillekens, L. Galdino, D. Semrau, R. Killey and P. Bayvel are with the Department of Electrical and Computer Engineering, University College London, London, WC1E 7JE UK.

A. Edwards, W. Pelouch and S. Barnes are with Xtera, Bates House, Church Road, Romford, RM3 0SD, UK (email: wayne.pelouch@xtera.com).

cation (> 5 THz), improved noise-figure allowing longer span lengths and reduced nonlinear penalty as a result of enabling a reduced signal launch power. The benefits of Raman amplification are well known, but not commonly used due to additional cost and the requirement of managing line connectors and losses at high optical power. In a submarine system, there are no connectors or poorly maintained fibre, so one of the main obstacles is overcome. Whilst Raman amplification remains more costly than an EDFA-only system, these costs are offset by longer span lengths, wider bandwidths, minimal increase in optical component count. Utilising the full amplification band of a high efficiency single-stage EDFA with the above advantages of DRA provides an interesting alternative solution for wideband high performance amplification. Such hybrid solutions exist and are commercially viable in repeatered submarine systems. In this paper, a hybrid Raman/EDFA (HRE) amplifier designed to achieve both wide-bandwidth and low noise-figure amplification is described, in conjunction with a new modulation scheme, demonstrating record data-rate transmission.

When designing transmission systems that maximise the achievable information rate, it is beneficial to combine the increase in transmission bandwidth with improvements in the SNR. Probabilistic [10] and geometric constellation shaping [14]-[17] enable the system achievable rate to be fine-tuned towards approaching the Shannon limit at a given SNR.

It has been theoretically demonstrated that, given a fixed number of constellation points, probabilistic shaping (PS) outperforms geometric shaping (GS) [18]. However, PS is commonly realised through a distribution matcher, whose hardware implementation is prohibitively complex for long block lengths or, which suffers a rate penalty for short block lengths [19]. Therefore, GS provides a more pragmatic approach, and hence we have applied it in this demonstration. In this paper, we have further optimised the GS constellation towards additionally mitigating transceiver impairments.

This paper is organised as follows: Section II describes the constituent parts of the transmission systems, including the hybrid amplifier, geometrically shaped modulation format and DSP techniques employed. Section III describes in detail the experimental setup and system performance, measured in terms of SNR, bit-wise AIR and post-FEC BER. Finally, in Section IV we present our conclusions.

## II. Subsystems

### A. Hybrid Raman/EDFA Amplification

The hybrid Raman/EDFA (HRE) amplifier design used in this experiment is shown schematically in Fig. 2. Each HRE comprised of single-stage EDFA pumped from a 980 nm pump and Raman backward pre-amplification stage from two 1427 nm and two 1495 nm pumps into the transmission fibre. The EDFA is pumped by a 980-nm pump, which provides most of the gain in the C-band with gain dropping to a small value at long wavelengths. The 1427-nm pump provides gain at the short wavelength side of the spectrum and additionally transfers pump power to the 1495-nm pump which provides most of the gain in the L-band. This configuration enables flexibility over the spectral tilt and gain shape of the amplifier. Each of the four Raman pumps operated with output powers of ≈ 300 mW, delivering a total signal power of 89 mW (19.5 dBm) to a second, EDFA-based amplification stage. A single 980 nm EDFA pump was operated at ≈ 550 mW output powers, providing a total signal output power of 158.5 mW (22 dBm). A gain-flattening filter is used at the output of the amplifier and has a peak attenuation of approximately 2.5 dB, enabling the gain ripple of each amplifier to be minimised down to ≈ 0.4 dB over 89 nm bandwidth.

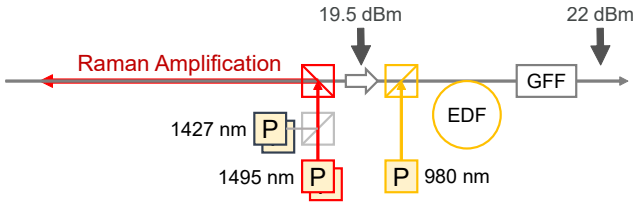


Fig. 2: Schematic of hybrid Raman/EDFA stages.

Fig. 3 shows the effective noise figure of the hybrid amplifier which is defined as the noise figure required by an equivalent EDFA to give the same output SNR and it is calculated as:

$$\mathrm{NF_{eff}} = \mathrm{NF_{meas.}} - \text{ Span Loss.}$$

A negative effective NF is not uncommon for HREs, as it is the case here for the upper L-band wavelengths. The amplifiers used in this experiment had an average $\overline{\mathrm{NF}}_{\mathrm{eff}} \approx 1.37$ dB, enabling 3 dB extra span loss, compared to the shorter spans of 52.8 - 55 km in similar types of experiments [8]-[9].

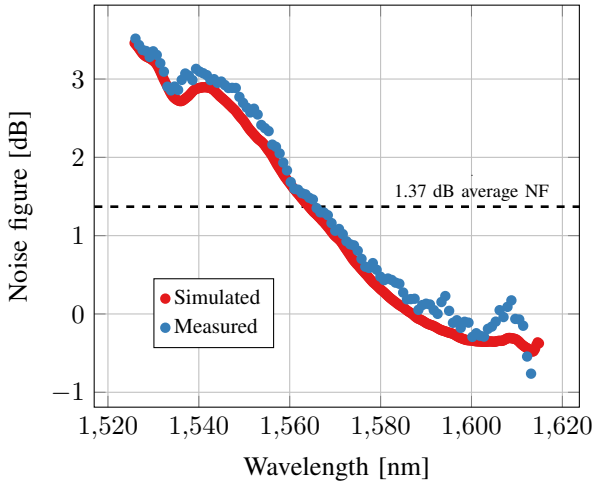


Fig. 3: Effective noise figure of the hybrid Raman/EDFA amplifier.

### B. Optimised Geometrically-Shaped Constellation Format

In this experiment we designed a GS 64QAM modulation format, tailored to the linear impairments of the transmission link and mitigating transceiver-induced nonlinear impairments. Starting from square 64QAM, the constellations at each optimisation stage are shown in Fig. 4. We chose the generalised mutual information (GMI) as the optimisation parameter.

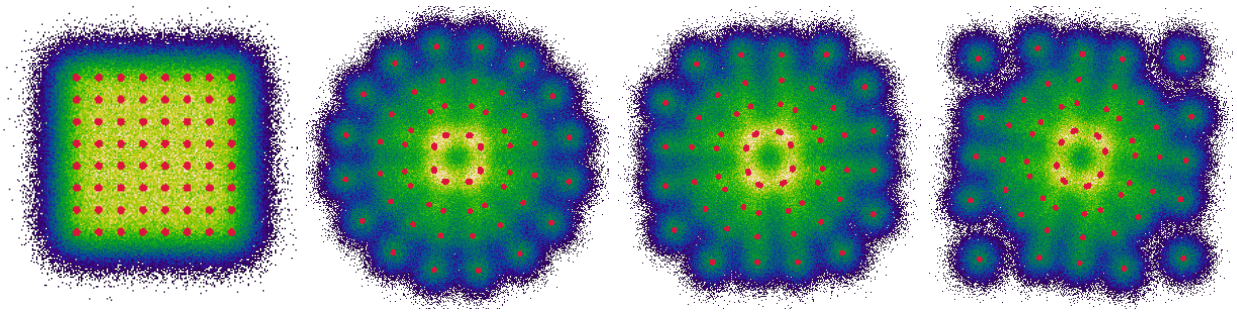

Fig. 4: Constellation diagrams of 64QAM for an SNR of 12 dB, after each optimisation stage, adding robustness against various impairments: (from left to right) standard square 64QAM, AWGN-optimised, joint AWGN+PAPR optimised, AWGN+PAPR optimised with outer markers for CPE.

The geometrically-shaped modulation format was designed by initially using a gradient descent algorithm with a cost function seeking to maximize GMI, an AIR of bit-wise receivers.

For a multi-dimensional AWGN channel, given $X$ transmitted symbols, the received symbols are

$$\mathbf{Y} = \mathbf{X} + \mathbf{Z}, \tag{1}$$

where $\mathbf{Z}$ represents the random noise vector. Given $m$ number of bits per symbol and $M = 2^m$ is the modulation cardinality, the GMI is defined as [20, Eq. (17,18)]:

$$G(\mathbf{X}, \sigma_{\mathbf{z}}) = m + \frac{1}{M} \sum_{k=1}^{m} \sum_{b \in \{0,1\}} \sum_{i \in I_k^b} \int_{\mathbb{C}^N} f_{\mathbf{Y}|\mathbf{X}}(\mathbf{y}|\mathbf{x}_i, \sigma_{\mathbf{z}}) \cdot \log_2 \frac{\sum_{j \in I_k^b} f_{\mathbf{Y}|\mathbf{X}}(\mathbf{y}|\mathbf{x}_j, \sigma_{\mathbf{z}})}{\sum_{p=1}^{M} f_{\mathbf{Y}|\mathbf{X}}(\mathbf{y}|\mathbf{x}_p, \sigma_{\mathbf{z}})} d\mathbf{y} \tag{2}$$

where $\mathbf{x} = [\mathrm{x}_I, \mathrm{x}_Q]^T \in \mathcal{X} \subset \mathbb{R}^2$, $\mathbf{y} = [\mathrm{y}_I, \mathrm{y}_Q]^T \subset \mathbb{R}^2$ are realisations of the random variables $\mathbf{X}$ and $\mathbf{Y}$ respectively, $\mathcal{X} = \{\mathbf{x}_1, \ldots, \mathbf{x}_M\}$ is the set of equiprobable constellation points. $I_k^b$ is the set of constellation points, associating the $k$-th bit to the bit value $b$. The channel law, defined as [20, Eq. (19)]

$$f_{\mathbf{Y}|\mathbf{X}}(\mathbf{y}|\mathbf{x}_i, \sigma_{\mathbf{z}}) = \frac{1}{\pi \sigma_{\mathbf{z}}^2} \cdot e^{-\frac{||\mathbf{y}-\mathbf{x}||^2}{\sigma_{\mathbf{z}}^2}} \tag{3}$$

depends on the SNR, which in turn is defined as the ratio between the variance of the transmitted symbols $\sigma_{\mathbf{x}}^2$ and the variance of the noise $\sigma_{\mathbf{z}}^2$:

$$\mathrm{SNR} = \frac{\sigma_{\mathbf{x}}^2}{\sigma_{\mathbf{z}}^2} = \frac{E\left[||\mathbf{X}||^2\right]}{E\left[||\mathbf{X} - \mathbf{Y}||^2\right]} \tag{4}$$

For the target SNR of 12 dB, we designed the GS-64QAM using the gradient-descent approach. Let $\mathbf{X}(n)$ be the current best solution, representing the set of symbols of our 64QAM constellation. The noise variance $\sigma_{\mathbf{z}}^2 = E\left[||\mathbf{Z}||^2\right]$ accounts for the ASE of the transmission link, which is fixed such that the SNR = 12 dB. We define and minimise the cost function:

$$J(X(n)) = -G(\mathbf{X}(n), \sigma_{\mathbf{z}}) \tag{5}$$

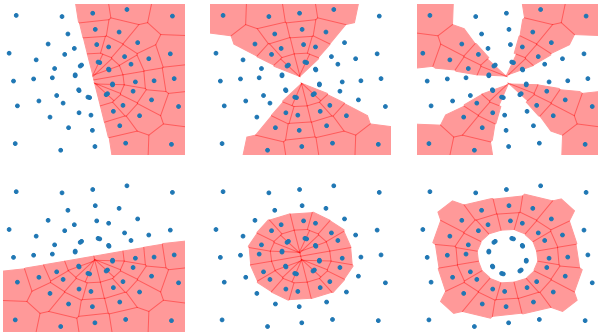

Fig. 5: GS-64QAM constellation optimised for transmission at 12 dB and labelling for each of the 6 bits. Shaded regions are the Voronoi regions for each bit for illustrative purposes only, no hard decisions are being made for the symbol. The shaded regions correspond to a zero being transmitted, the open region to one.

The symbols are iteratively adjusted on the complex constellation plane, such that the cost function is minimised, leading to a maximisation of the GMI:

$$\mathbf{X}(n+1) = \mathbf{X}(n) - \frac{\mu}{2} \nabla J(\mathbf{X}(n)) \tag{6}$$

where $\mu$ is the gradient-descent step-size.

The resulting constellation produced an equivalent GMI to the formats designed in [15] (second constellation in Fig. 4). The bit labelling derivation is a travelling salesmen problem, where all pair-wise swaps between constellation points are tested every few iterations of the gradient descent. We show the final constellation shape and the bit decision regions in Fig. 5. The algorithm forces the 16 constellation points of the inner ring to be almost overlapping, leaving the constellation format appearing to have only 56 symbols. The format is thus 64QAM where at an SNR of 12 dB there is no information transmitted in the transition between every 2 symbols of the inner ring.

The results of the numerical optimisation has 16 constellation points of the inner ring to be almost overlapping, leaving the constellation format appearing to have only 56 symbols. However, for every symbol, there are still 64 coordinates with 64 bit labels, allowing the bit demapping to be done

with off-the-shelf soft-demapping algorithms. The optimised constellations would be different for each channel, although in this experiment we used the same modulation format across the entire transmission bandwidth, despite the SNR fluctuations from channel to channel of $\approx$ 2 dB over 95% of the wavelengths. The GMI improvement of GS-64QAM compared to 64QAM at the target SNR=12 dB is 0.34 bit/4D-symbol.

The constellation that has been optimised for the AWGN channel has quite a high peak-to-average power ratio (PAPR) by comparison to the square 64QAM format. A high PAPR generally incurs nonlinear signal distortions [16] from the transmitter elements i.e. DAC, modulator, as well as the transmission fibre, which would therefore result in the transmitted constellations having a lower SNR. Therefore, we further modified the modulation format optimisation algorithm to tailor the constellations for obtaining a lower PAPR. To achieve this, we redefined the gradient-descent cost function to take into account the impact of the PAPR as an additional constraint in the noise variance:

$$J(X(n)) = -G\Bigg(\mathbf{X}(n), \sigma_{\text{AWGN}} + \left(\frac{\max(|\,\mathbf{X}(n)\,|^2)}{E\left[||\,\mathbf{X}(n)\,||^2\right]} - \frac{\max(|\,\mathbf{X}_{64}\,|^2)}{E\left[||\,\mathbf{X}_{64}\,||^2\right]}\right)\cdot\sigma_{\text{PAPR}}\Bigg) \tag{7}$$

where $\mathbf{X}_{64}$ is the set of symbols corresponding to the square 64QAM modulation format. The resulting constellation is the third constellation in Fig. 4. The PAPR-induced SNR penalty has been included as a linear noise contribution, $\sigma_{\text{PAPR}}$ scaled with the difference in PAPR from regular 64QAM, along with the AWGN noise component $\sigma_{\text{AWGN}}$. We define $\max(|\cdot|^2)$ as the maximum of the individual in-phase and quadrature components of all points. The constraint of Eq. 7 accounted for the transceiver nonlinearities, similarly to [17], but did not take into account the fibre-induced nonlinear interference. This modification avoids the extra GMI penalty (Fig. 6), that would have thus incurred from the SNR reduction, in the practical transmission system.

Finally, the amplitude of the four outer constellation points were increased to form a distinct ring, enabling their use as markers for blind carrier phase estimation (CPE) DSP [21]. This final adjustment led to the fourth constellation in Fig. 4, which was used in the experiment. The resulting GMI improvement of the system-tailored GS-64QAM compared to square 64QAM at the target SNR=12 dB is 0.25 bit/4D-symbol. Thus, the optimisation brought by CPE incurred a penalty of approximately 0.09 bit/4D-symbol compared to GS-64QAM.

### C. Digital Signal Processing

The DSP used in this work was designed to mitigate for both intra-channel nonlinear and linear impairments. For nonlinear compensation, the channel of interest was digitally backpropagated (DBP) over 4 steps per span, to ensure a trade-off between performance and complexity. DBP brings an

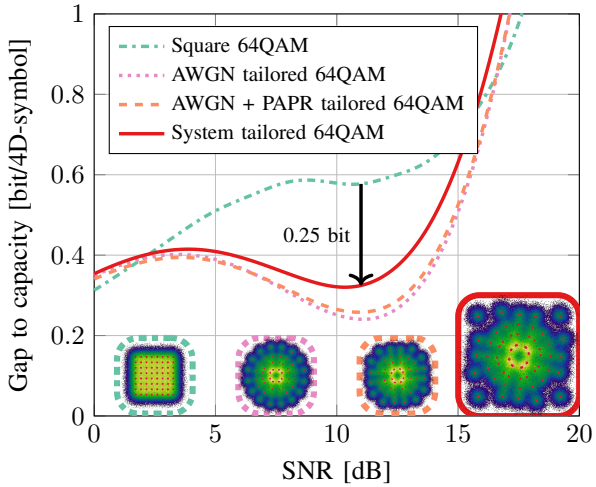


Fig. 6: GMI gap to capacity per 4D-symbol for modulation formats optimised for 12 dB received SNR.

average improvement of $\approx$ 0.4 dB to the receiver SNR. After nonlinear mitigation, the DSP stages are applied in this order: RRC matched filtering with roll-off of 1% and bandwidth 60 GHz to enable signal alignment, despite the presence of a frequency offset, 19-taps radially-directed equaliser, frequency offset compensation and carrier phase estimation (CPE) based on Viterbi & Viterbi with a window of 512 samples. The latter stage was enabled by the outer four constellation points from the system tailored GS-64 QAM constellation, which however induced a GMI penalty, as outlined in Section II-B. However, the estimated data-rate loss for GS-64QAM with system tailored CPE markers is 0.7% which is significantly lower than the typical $3-10\%$ required by pilot-aided CPE [22]. In many practical systems blind-phase search CPE [23] is applied, however at the cost of increased DSP complexity. In this case, the rate loss of 0.7% induced by the outer constellation markers would be avoided. However, for the purpose of reducing the implementation complexity in our DSP, we have opted for the Viterbi & Viterbi CPE instead.

Finally, the channels were decoded using 9 rate adapted LDPC codes implemented from the DVB-S2x [24]. The overheads values were between 55% and 200%. A outer BCH HD-FEC with 0.5% overhead was assumed when quantifying the BER performance, which would then lower the post-HD-FEC BER to below $10^{-15}$. Whilst the KP4 FEC i.e. RS(544, 514) is chosen for its low complexity, we have chosen the FEC codewords length much closer to the 64000 of the DVBS2 FEC codewords, i.e., BCH(65535, 65231) which corrects up to 19 errors resulting in 0.466% OH with a threshold of $2.8992\cdot10^{-4}$, rounded to 0.5% and $3\cdot10^{-4}$ respectively.

## III. Performance Analysis

### A. Experimental Setup

The experimental setup is shown in Figure 7. The transmitter consisted of two parts: an ASE noise source and four modulated channels. Spectral noise loading has been previously demonstrated to give pessimistic performance results

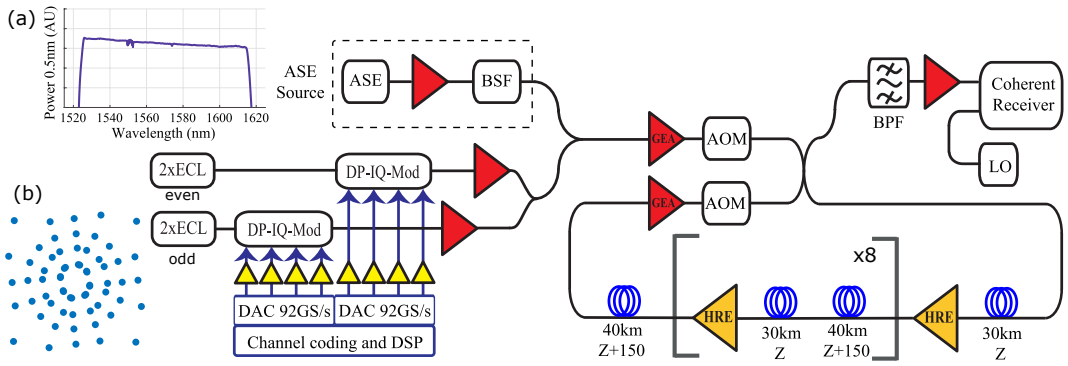


Fig. 7: Experimental setup and insets of (a) constellation diagram of system-tailored DP-GS64QAM and (b) transmitted spectrum. Amplifiers shown in red are DRAs for signal boosting; amplifiers shown in yellow are the hybrid Raman/EDF amplifiers

compared to the use of modulated channels across the full transmission bandwidth [25]. As such, the performance of our system could be considered as a lower-bound with respect to conventional channel loading. The ASE noise source generated by a set of DRAs covered a continuous total bandwidth of 97 nm; this was followed by a band-stop filter (BSF) for creating a spectral gap at the location where the channels of interested were inserted. The filter used (Yenista WSM-160) had >40 dB rejection ratio with adjustable FWHM bandwidth between 0.25 nm to 60 nm and a flatness of 0.3 dB; The four test channels generated from four independent lasers and modulated as pairs of odd/even channels by two independent dual-polarisation IQ modulators. The lasers were set on a 35.5 GHz grid and jointly swept from 1525.56 nm to 1614.54 nm, allowing the measurement of 306 channels, covering a total continuous spectrum of 89 nm. Two independent 92 GSa/s digital-to-analogue converters (DACs) were used to drive the IQ modulators at a baud-rate of 35 GBaud with the optimised GS-64QAM modulation format, interleaved to generate two sets of odd and even channels. Each channel was Nyquist pulse shaped with a root-raised cosine (RRC) filter of 1% roll-off factor. The channel powers were boosted with DRAs of 12.5 dB gain, prior to being multiplexed with the ASE noise source. An additional gain-equalising amplifier (GEA), comprising a discrete Raman amplification stage followed by a digital equalising filter, was used to pre-amplify and spectrally shape the combined signal prior to transmission. A power tilt of approximately -2 dB across the bandwidth was applied to optimize channel performance, taking into account the wavelength-dependent noise figure of the transmission line amplifiers.

The recirculating loop comprised of 9 x 70 km fibre spans. Within each span, the first 40 km used high-effective core area fibre (Sumitomo Z+, $A_{\text{eff}} = 150\ \mu\text{m}^2$) to lower the nonlinear effects experienced by the signals due to the high power at the beginning of the fibre, with the remaining 30 km using low-loss, terrestrial-standard core size fibre (Sumitomo Z, $A_{\text{eff}} = 80\ \mu\text{m}^2$) to increase the Raman gain provided by the backward propagating pumps of the HRE. The total span loss was approximately 10.72 dB. After each recirculation, a second GEA was used to reshape the signal spectrum and partially correct the cumulative gain ripple from the cascaded HRE chain. The gain of the GEA was also used to compensate for the loss of the gain equalizing dynamic filter and AOM switch. The GEA contains a discrete Raman gain fibre which has a smaller effective area than the line fibre and thus a higher nonlinear coefficient. For this reason, this amplifier was placed in the middle of the span where the signal power was lower, thus ensuring minimal additional nonlinear penalties. After 10 recirculations covering a total transmission distance of 6,300 km, a band-pass filter (BPF) of around 35.5 GHz bandwidth was used at the receiver-end to select one of the inner channels from the four channel group for decoding and system performance measurements. The polarisation and phase diverse coherent receiver incorporated 70 GHz bandwidth photodetectors, and the signal was digitised using a four-channel real-time oscilloscope with a 63 GHz electrical bandwidth, sampling at 160 GSa/s. The Osciloscope captured 131,072 symbols for off-line DSP.

In qualifying the performance of the system, we first analyse the SNR after transmission and then we show both the AIR and BER after SD-FEC decoding.

### *B. SNR Performance*

Figure 8 shows the SNR calculated from the constellation points at the receiver after applying DBP. The receiver SNR was obtained by evaluating Eq. 4. The average SNR thus obtained in the experiment is 11.1 dB before DBP and 11.5 dB after DBP, giving an average 0.4 dB performance improvement brought by the nonlinear mitigation stage. The L-band channels generally operate at a slightly higher than average SNR and this improvement could be attributed mainly to their associated lower noise figure and the SRS gain given by the C-band channels. While the contributions of the link to the degradation of the SNR dominate, the back-to-back SNR is equivalent to 2 recirculations i.e., 19.6 dB. Therefore, any improvements to the transceiver SNR could provide further performance gains, but this would be non-trivial given the high insertion losses of the modulators.

The calculated SNRs show higher penalties at the edge wavelengths due to loop components filtering (i.e., AOMs, GFFs), which was not included in the model.

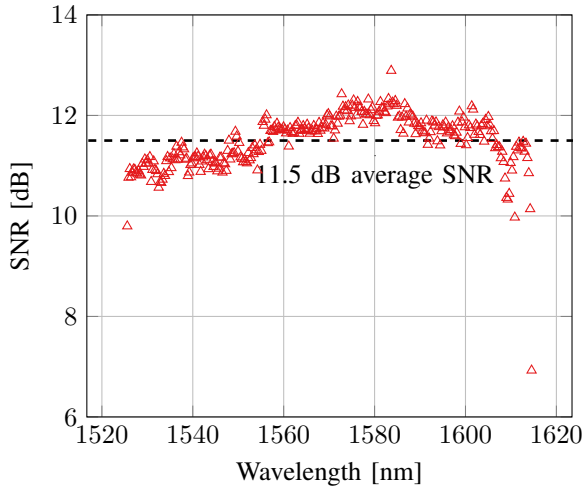


Fig. 8: Experimental SNR obtained after 6300 km and digital nonlinear mitigation.

### C. Achievable Information Rates

Figures 9 and 10 show the per channel bit-wise AIRs and BERs respectively, before and after FEC. While only the SD-FEC decoding was implemented, the AIR we show in Figure 9 takes into account the assumed 0.5% HD-FEC overhead. When using SD-FEC, there is no bit decision made on the pre-FEC bits. Instead, the log-likelihood ratios are calculated according to [20, Eq. (23)] . The discrete levels of the net channel-rates are a direct result of the 9 distinct LDPC code-rates used in the SD-FEC implementation. The slight penalty around 1610 nm, equally observed in both AIR and post-FEC rates, could be attributed to higher nonlinearity penalties induced by the peak Raman gain of the 1495 nm pump, where the DBP didn't give significant gains.

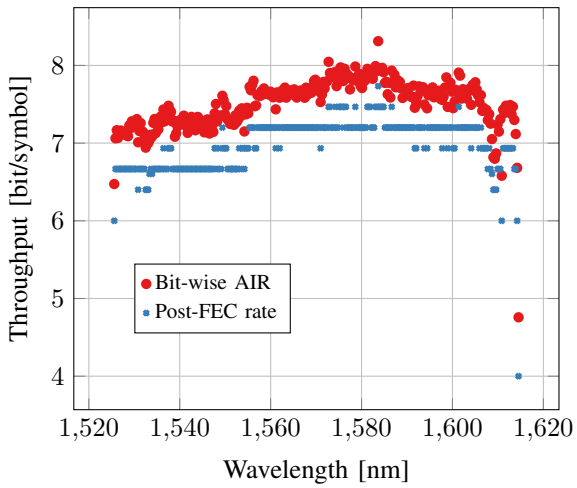


Fig. 9: Throughput per channel over 2 polarisations after transmission over 6300 km.

The BER is shown before and after SD-FEC implementation in Figure 10, with all channels performing within the HD-FEC limit after the SD-FEC has been employed.

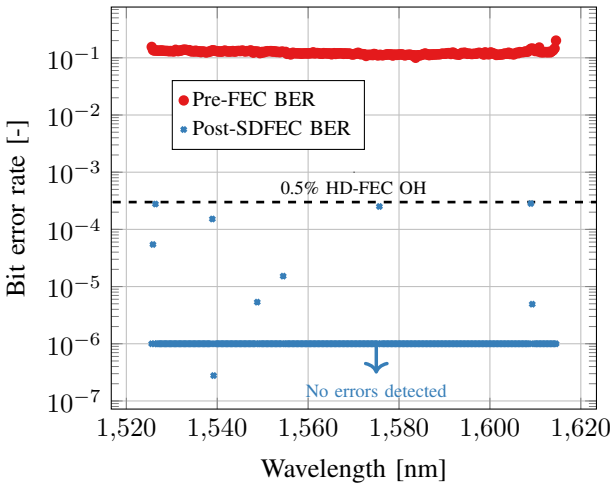


Fig. 10: Pre-FEC and post-SD-FEC BER for all 306 channels.

In Figure 11 we assess the capacity obtained in this paper of 74.38 Tb/s over 6,300 km against the Shannon's AWGN channel capacity limit $C = 2{\cdot}B{\cdot}\log_2(1{+}\text{SNR})$, given bandwidth of the transmission system presented here $B = 10.86$ THz. The gap is calculated both in relation to the difference in capacity between the predicted limit at the average SNR of the system, as well as the the SNR difference at the attained capacity of the system. The gap to capacity is approximately 10.7 Tb/s due to a combination of penalties. From this total loss in capacity, approximately 4 Tb/s can be accounted for by the non-Gaussian modulation format, despite having tailored the constellation close to the system's average SNR and optimised for minimum PAPR penalties. The remaining loss in capacity is due to LDPC penalties, resulting from an implementation over a fixed range of code-rates, which could be improved by better codes instead of standard implementable codes. In terms of the SNR gap, we see 1.6 dB difference from the Shannon limit. This is due to transceiver and link penalties (i.e. linear and nonlinear impairments, amplifier gain ripples, transceiver SNR, DSP penalties) which we cannot analytically account for. Improving the SNR of the experimental setup would therefore be desirable to reducing the gap to Shannon's limit.

For comparison we also plot the previous transmission capacity of 120 Tb/s over 630 km of our previous experiment based on the same setup [26]. This experiment was over a short distance, equal to a single loop recirculation. The principal difference in setup was the omission of the loop controlling equipment and the extra loop GEA, used for loop losses and reducing the gain ripple. In this experiment, the penalty in capacity is even higher than in the long-haul setup, primarily as a result of employing 256-QAM modulation. Despite a higher SNR of 18.8 dB, the AIR gap to Shannon is 0.94 bit/symbol. By contrast, when employing the optimised GS-64QAM format in the long-distance experiment, a penalty of 0.33 bit/symbol was obtained at SNR 12 dB. The SNR gap of 2.3 dB is also higher comparing the short-distance to the long-distance experiments. The slight difference in setup, such as the extra GEA loop amplifier, choice of modulation format, higher impact of transceiver SNR on short-distance

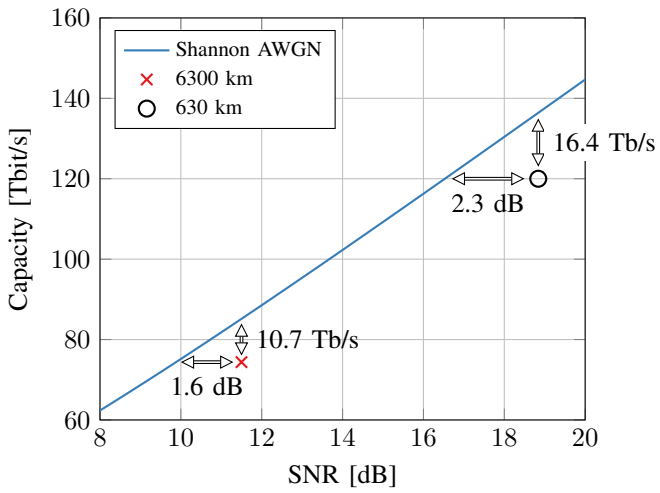


Fig. 11: The gap to Shannon's AWGN channel capacity, i.e., $2B\log_2(1+SNR)$, with bandwidth $B$=10.86 THz.

experiments, can account for this gap increase. Therefore, contrasting the two experiments, we show that despite increasing the transmission distance which incurred its respective and expected impact on the total capacity, the performance of the long distance system with respect to the linear channel limit is greatly improved, notably through the optimisation of the modulation format.

## IV. Conclusion

In this paper we presented a high capacity record result over $6,300$ km of SMF, employing C+L transmission by using hybrid Raman/EDF amplifiers, system-tailored, geometrically shaped, modulation format, single channel DBP for nonlinearity mitigation and rate-adaptive SD-FEC decoding. The continuous $\approx 89$ nm bandwidth of the amplifiers used in this experiment enables an additional $11$ nm ($\approx 12\%$ bandwidth expansion) overall compared to C+L EDFA only solution [8]. The Raman pumps allow fine tailoring of spectral gain (i.e., tilt control) and a reduced noise-figure which in turn result in 3 dB longer span lengths. A total of 74.38 Tb/s was transmitted over 6300 km of combined Sumitomo Z+150 and Z fibres. Whilst the highest capacity gains come from the extended amplifier bandwidth, additional benefits come from the received SNR improvements achieved by employing a system-tailored GS-64QAM format and DBP. The non-ideal modulation formation still leads to $\approx 4$ Tb/s gap to Shannon capacity while the SD-FEC implementation results in a further $\approx 6$ Tb/s penalty. However, these results show that significant improvements could be brought to the AIR transoceanic systems, based on SMF, through careful optimisation of all the constituent subsystems.

## Acknowledgment

The authors are grateful to Steve Desbruslais for fruitful discussions, Bin Chen and Alex Alvarado from Eindhoven University of Technology for valuable feedback on the manuscript, Finisar and Sumitomo for their support in this investigation and Oclaro for the modulators. EPSRC funding (EP/R035342/1, TRANSNET) is gratefully acknowledged. E. Sillekens is supported by EPSRC (EP/M507970/1) and Xtera Inc. L. Galdino and D. Lavery are supported by the Royal Academy of Engineering under the Research Fellowships scheme.

## References

[1] J.-X. Cai, C. R. Davidson, A. Lucero, H. Zhang, D. G. Foursa, O. V. Sinkin, W. W. Patterson, A. N. Pilipetskii, G. Mohs, and N. S. Bergano, "20 Tbit/s Transmission Over 6860 km With Sub-Nyquist Channel Spacing," J. Lightwave Technol. 30, 651-657 (2012)

[2] M. Mazurczyk, D. G. Foursa, H. G. Batshon, H. Zhang, C. R. Davidson, J. -. Cai, A. Pilipetskii, G. Mohs, and N. S. Bergano, "30 Tb/s Transmission over 6,630 km Using 16QAM Signals at 6.1 bits/s/Hz Spectral Efficiency," in European Conference and Exhibition on Optical Communication, OSA Technical Digest (online) (Optical Society of America, 2012), paper Th.3.C.2.

[3] D. G. Foursa et al., "44.1 Tb/s transmission over 9,100 km using coded modulation based on 16QAM signals at 4.9 bits/s/Hz spectral efficiency," 39th European Conference and Exhibition on Optical Communication (ECOC 2013), London, 2013, pp. 1-3.

[4] J.-X. Cai, Y. Sun, H. Zhang, H. G. Batshon, M. V. Mazurczyk, O. V. Sinkin, D. G. Foursa, and A. Pilipetskii, "49.3 Tb/s Transmission Over 9100 km Using C+L EDFA and 54 Tb/s Transmission Over 9150 km Using Hybrid-Raman EDFA," J. Lightwave Technol. 33, 2724-2734 (2015)

[5] J. Cai et al., "51.5 Tb/s Capacity over 17,107 km in C+L Bandwidth Using Single-Mode Fibers and Nonlinearity Compensation," in Journal of Lightwave Technology, vol. 36, no. 11, pp. 2135-2141, 1 June1, 2018.

[6] J. -. Cai et al., "54 Tb/s transmission over 9,150 km with optimized hybrid Raman-EDFA amplification and coded modulation," 2014 The European Conference on Optical Communication (ECOC), Cannes, 2014, pp. 1-3.

[7] J. X. Cai, H. G. Batshon, M. Mazurczyk, H. Zhang, Y. Sun, O. V. Sinkin, D. G. Foursa, and A. Pilipetskii, "64QAM Based Coded Modulation Transmission over Transoceanic Distance with ¿ 60 Tb/s Capacity," in Optical Fiber Communication Conference Post Deadline Papers, OSA Technical Digest (online) (Optical Society of America, 2015), paper Th5C.8.

[8] J. Cai, H. G. Batshon, M. V. Mazurczyk, O. V. Sinkin, D. Wang, M. Paskov, W. W. Patterson, C. R. Davidson, P. C. Corbett, G. M. Wolter, T. E. Hammon, M. A. Bolshtyansky, D. G. Foursa, and A. N. Pilipetskii, "70.46 Tb/s Over 7,600 km and 71.65 Tb/s Over 6,970 km Transmission in C+L Band Using Coded Modulation With Hybrid Constellation Shaping and Nonlinearity Compensation," *J. Lightw. Technol*, vol. **36**, no. 1, pp. 114-121 (2018).

[9] A. Ghazisaeidi et al., "65Tb/s Transoceanic Transmission Using Probabilistically-Shaped PDM-64QAM," ECOC 2016 - Post Deadline Paper; 42nd European Conference on Optical Communication, Dusseldorf, Germany, 2016, pp. 1-3.

[10] A. Ghazisaeidi, I. F. de Jauregui Ruiz, R. Rios-Mller, L. Schmalen, P. Tran, P. Brindel, A. C. Meseguer, Q. Hu, F. Buchali, G. Charlet, and J. Renaudier, "Advanced C+L-Band Transoceanic Transmission Systems Based on Probabilistically Shaped PDM-64QAM," in *J. of Lightw. Technol.*, vol. 35, no. 7, pp. 1291-1299, 1 April, 2017.

[11] M. Ionescu, D. Lavery, A. Edwards, E. Sillekens, L. Galdino, D. Semrau, R. I. Killey, W. Pelouch, S. Barnes, and P. Bayvel, "74.38 Tb/s Transmission Over 6300 km Single Mode Fiber with Hybrid EDFA/Raman Amplifiers," in Optical Fiber Communication Conference (OFC) 2019, OSA Technical Digest (Optical Society of America, 2019), paper Tu3F.3.

[12] J. Renaudier, A. C. Meseguer, A. Ghazisaeidi, P. Tran, R. Rios-Muller, R. Brenot, A. Verdier, F. Blache, K. Mekhazni, B. Duval, H. Debregeas, M. Achouche, A. Boutin, F. Morin, L. Letteron, N.s Fontaine, Y. Frignac, G. Charlet, "First 100-nm Continuous-Band WDM Transmission System with 115Tb/s Transport over 100km Using Novel Ultra-Wideband Semiconductor Optical Amplifiers," in *Proc. Eur. Conf. on Opt. Commun.* 2017, pp. 1-3.

[13] M. N. Islam, "Raman amplifiers for telecommunications," in IEEE Journal of Selected Topics in Quantum Electronics, vol. 8, no. 3, pp. 548-559, May-June 2002.

[14] S. Zhang, F. Yaman, Y. Huang, J. D. Downie, D. Zou, W. A. Wood, A. Zakharian, R. Khrapko, S. Mishra, V. Nazarov, J. Hurley, I. B. Djordjevic, E. Mateo, and Y. Inada, "Capacity-approaching transmission over 6375 km at spectral efficiency of 8.3 bit/s/Hz", in *Proc. Opt. Fiber Commun. Conf.*, 2016.

[15] B. Chen, C. Okonkwo, H. Hafermann and A. Alvarado, "Increasing Achievable Information Rates via Geometric Shaping," in *Proc. Eur. Conf. on Opt. Commun.* 2018, We1F.4.

[16] A. Mecozzi and R. Essiambre, "Nonlinear Shannon Limit in Pseudo-linear Coherent Systems," in *J. Lightw. Technol.*, vol. **30**, no. 12, pp. 2011-2024 (2012).

[17] E. Sillekens, D. Semrau, D. Lavery, P. Bayvel and R. I. Killey, "Experimental Demonstration of Geometrically-Shaped Constellations Tailored to the Nonlinear Fibre Channel," in *Proc. Eur. Conf. on Opt. Commun.* 2018, Tu3G.3.

[18] F. Steiner and G. Boecherer, "Comparison of geometric and probabilistic shaping with application to ATSC 3.0," in 2017 International ITG Conference on Systems, Communications and Coding (SCC), Feb 2017, pp. 16.

[19] G. Bocherer, F. Steiner, and P. Schulte, "Fast probabilistic shaping implementation for long-haul fiber-optic communication systems," in 2017 European Conference on Optical Communication (ECOC), Sep. 2017, pp. 13.

[20] A. Alvarado, T. Fehenberger, B. Chen, and F. M. J. Willems, "Achievable Information Rates for Fiber Optics: Applications and Computations," *J. Lightw. Technol.*, vol. **36**, no. 2, pp. 424-439 (2018).

[21] A. Viterbi, "Nonlinear estimation of PSK-modulated carrier phase with application to burst digital transmission," in IEEE Transactions on Information Theory, vol. 29, no. 4, pp. 543-551, July 1983.

[22] M. Magarini et al., "Pilot-Symbols-Aided Carrier-Phase Recovery for 100-G PM-QPSK Digital Coherent Receivers," in IEEE Photonics Technology Letters, vol. 24, no. 9, pp. 739-741, May1, 2012.

[23] T. Pfau, S. Hoffmann and R. Noe, "Hardware-Efficient Coherent Digital Receiver Concept With Feedforward Carrier Recovery for $M$ -QAM Constellations," in Journal of Lightwave Technology, vol. 27, no. 8, pp. 989-999, April15, 2009.

[24] European Telecommunications Standards Institute, "Digital Video Broadcasting (DVB): Part 2: Extensions," ETSI EN 302 307-2.

[25] D. J. Elson, G. Saavedra, K. Shi, D. Semrau, L. Galdino, R. Killey, B. C. Thomsen, and P. Bayvel, "Investigation of bandwidth loading in optical fibre transmission using amplified spontaneous emission noise," in Opt. Express 25, 19529-19537 (2017).

[26] M. Ionescu et al., "91 nm C+L Hybrid Distributed RamanErbium-Doped Fibre Amplifier for High Capacity Subsea Transmission," 2018 European Conference on Optical Communication (ECOC), Rome, 2018, pp. 1-3.